



ELSEVIER

Contents lists available at ScienceDirect

Journal of Hydrology

journal homepage: www.elsevier.com/locate/jhydrol

Research papers

Identification of groundwater basin shape and boundary using hydraulic tomography

Kwankwai Daranond^a, Tian-Chyi Jim Yeh^{a,b,*}, Yonghong Hao^b, Jet-Chau Wen^{c,d}, Wenke Wang^e

^a University of Arizona, Department Hydrology and Atmospheric Sciences, Tucson, AZ, USA

^b Tianjin Key Laboratory of Water Resources and Environment, Tianjin Normal University, Tianjin, China

^c Department of Safety, Health, and Environmental Engineering, National Yunlin University of Science and Technology, Douliu, Taiwan

^d Research Center for Soil and Water Resources and Natural Disaster Prevention, National Yunlin University of Science and Technology, Douliu, Taiwan

^e Key Laboratory of Subsurface Hydrology and Ecological Effects in Arid Region, Chang'an University, Xi'an, China

ARTICLE INFO

Keywords:

Hydraulic Tomography (HT)
 Aquifer bedrock geometry
 Impermeable and constant head boundaries
 Prior information
 Heterogeneity

ABSTRACT

Shapes and boundary types of a groundwater basin play essential roles in the analysis of groundwater management and contaminant migration. Hydraulic tomography (HT), a recently developed new approach for high-resolution characterization of aquifers, is not only an inverse method but a logical strategy for collecting non-redundant hydraulic information. In this study, HT was applied to synthetic 2-D aquifers to investigate its feasibility to map the irregular shapes and types of the aquifer boundaries. We first used the forward model of VSFT2 to simulate hydraulic responses due to HT surveys in the aquifer with irregular geometry and pre-determined constant head conditions at some boundaries, and no-flow conditions at others. The SimSLE (Simultaneous Successive Linear Estimator) inverse model in VSFT2 was then used to interpret the simulated HT data to estimate the spatial distribution of hydraulic properties of the aquifer using a domain with a wrong geometry surrounded by boundaries of a constant head condition. The inverse modeling experiment used steady-state and transient-states data from the HT forward simulations, and it used the same monitoring network as in the aquifer with irregular geometry to assess the ability of HT for detecting types and shapes of the boundary as well as heterogeneity in the aquifer. Results of the experiment show that no-flow boundaries, which were incorrectly treated as constant head boundaries in inverse models, were portrayed as low permeable zones of the aquifer near the boundaries. Overall, the results show that HT could delineate not only the irregular shape of the aquifer in general but also heterogeneity in the aquifer. Improvements of the estimation with prior information of transmissivity and storage coefficient was also investigated. The study shows that using homogeneous initial guess parameters resulted in a slightly better estimate than others. Moreover, this study employs Monte Carlo simulations to ensure statistically meaningful conclusions.

1. Introduction

Proper management and protection of groundwater resources require detailed aquifer characterization. Over the past few decades, the conventional pumping test analyses, such as methods by Theis (1935) and by Cooper and Jacob (1946), have been widely adopted to estimate the aquifer characteristics. They are parsimonious, but they do not provide sufficient information for a high-resolution understanding and prediction of flow and contaminant transport processes (Wu et al., 2005).

Recently, a new method of aquifer test and analysis (i.e., Hydraulic Tomography, HT) has been developed (see Yeh and Liu, 2000; Zhu and Yeh, 2005; Xiang et al., 2009). It involves successively conducting a

pumping test at a well and monitoring aquifer responses at others in a well field until the test is completed at all selected pumping wells. Such test data are then analyzed using a highly parameterized inverse model to estimate detailed spatial distributions of hydraulic parameters of the aquifer. HT, in essence, gathers aquifer responses from a limited number of wells under different flow fields. These responses contain non-redundant information about aquifer heterogeneity such that the inverse modeling of heterogeneity is improved (Wen et al., 2019). Because of this new aquifer characterization approach, Yeh and Lee (2007) championed the time to change our approach to characterize aquifers. Over the past decades, many studies have validated HT's robustness, for examples, synthetic aquifers (Yeh and Liu, 2000; Zhu and Yeh, 2005; Ni et al., 2009; Bohling and Butler, 2010; Castagna et al.,

* Corresponding author at: University of Arizona, Department Hydrology and Atmospheric Sciences, Tucson, AZ, USA.

E-mail address: www.tian@hwr.arizona.edu (T.-C.J. Yeh).

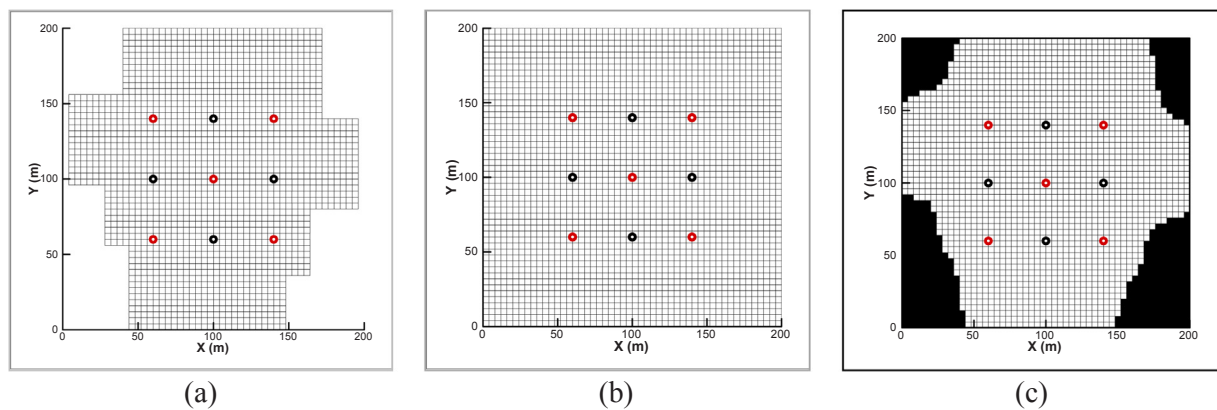


Fig. 1. Model geometry of (a) a synthetic aquifer and Case 1, (b) Case 2, and (c) Case 3.

2011; Tso et al., 2016), laboratory sandboxes (Liu et al., 2002; Liu et al., 2007; Yin and Illman, 2009; Berg and Illman, 2011; Illman et al., 2015; Zhao et al., 2016), and field aquifers (Straface et al., 2007; Wen et al., 2010; Cardiff and Barrash, 2011; Huang et al., 2011; Berg and Illman, 2013, 2015; Cardiff et al., 2012; Zha et al., 2016; Zhao and Illman, 2017, 2018).

While HT is useful, efforts to improve it have been proposed. For instance, the geological knowledge is employed as prior information to improve the heterogeneity estimation as discussed by Zhao et al. (2016), Zha et al. (2017), Zhao and Illman (2017, 2018) and Li et al. (2019). Likewise, transient HT has been developed (e.g., Zhu and Yeh, 2005; Xiang et al., 2009), but few studies have investigated the role of storage coefficient (S) or specific storage (Ss) on the aquifer characterization using HT. For instance, Tiedeman and Barrash (2019) mainly focused on hydraulic conductivity (K) estimation. Cardiff and Barrash (2011) combined the knowledge of geological data with HT and investigated the effect of S on the heterogeneity characterization. Cardiff et al. (2011) stated that the spatial variability of Ss would not have a large effect on estimated K as long as the information of Ss is reasonable. However, Castagna et al. (2011) and Sun et al. (2013) advocates the impacts of information of S on the estimation of transmissivity (T) and S.

Similarly, geologic features (such as bedrocks, mountains, and faults) often surround or cut through field aquifers, and their locations and hydraulic properties are generally unknown. Previous HT studies used synthetic aquifers or laboratory sandboxes where boundaries are known precisely. Such certainty about boundary conditions likely minimizes the uncertainty in the HT estimation. Few studies have investigated the effects of these unknown boundaries on the HT estimates. For example, Sun et al. (2013) examined the relationship between drawdown and aquifer properties, including the effect of using incorrect boundaries in the synthetic aquifers. They showed that the use of constant head boundaries in the inverse model could yield low permeability zones near the impermeable boundary of the true model. As such, they suggested using a constant head boundary for the unknown boundaries during HT analysis.

On the other hand, the application of HT to field aquifers undoubtedly involves uncertainty. To reduce the effects of the uncertain boundary conditions in field aquifers, previous studies (e.g., Straface et al., 2007; Cardiff et al., 2013; Lu et al., 2012; Illman et al., 2009; Zha et al., 2016) employed a large simulation domain compared to the size of the well-field. They then assigned some assumed boundary conditions to the boundaries.

Nonetheless, unknown geologic boundaries may exist near the well field and impact the HT estimates. Recently, the effects of the incorrect boundary conditions in synthetic aquifers were explored by Sun et al. (2013). They considered a single heterogeneous rectangular domain with a well field far from boundaries. They reported that HT could map

the impermeable boundary at far distances. Nevertheless, Wang et al., 2019, emphasized that HT results based on one single realization of synthetic heterogeneous aquifers may not be conclusive. Further, few studies have thoroughly investigated the effects of the irregular boundary shape on the estimation.

In this study, we apply HT to a synthetic heterogeneous aquifer for imaging the geometry of boundary and determine associated basin boundary conditions. We also investigate the effect of incorrectly assigned boundary conditions on the parameter estimates within the aquifer. Moreover, the impact of prior information of the storage coefficient on estimated T and S are examined. We employ Monte Carlo simulations to obtain representative results.

2. Methodology

2.1. Governing flow equation

This study uses VSATF2 (Variably Saturated Flow and Transport in two dimensions) (Yeh et al., 1993) to simulate a two-dimensional, horizontal groundwater flow model for saturated, heterogeneous media. The following partial differential equation describes the flow of groundwater,

$$\nabla \cdot [T(\mathbf{x}) \nabla H] + Q(\mathbf{x}_p) = S(\mathbf{x}) \frac{\partial H}{\partial t} \quad (1)$$

which is dependent on the boundary and initial conditions,

$$H|_{\Gamma_1} = H_1, [T(\mathbf{x}) \nabla H] \cdot \mathbf{n}|_{\Gamma_2} = q, \text{ and } H|_{t=0} = H_0 \quad (2)$$

where $T(\mathbf{x})$ is the transmissivity [L^2/T], H is the total head [L], $Q(\mathbf{x}_p)$ is the pumping rate [L^3/T] at location \mathbf{x}_p , $S(\mathbf{x})$ is the storage coefficient [-], H_1 is the prescribed total head at Dirichlet boundary Γ_1 , q is the prescribed flux at the Neumann boundary Γ_2 , \mathbf{n} is a unit vector normal to the boundary, and H_0 is the total head before applying any stress to the aquifer.

3. Forward reference model setup

In this study, a 2-D synthetic aquifer, representing a buried-valley aquifer with impermeable bedrocks with irregular shapes on the two sides (Fig. 1a), is considered. The aquifer is 200 m long from top to bottom, with a maximum width of 192 m from left to right. We discretize the aquifer into 1815 equal size finite element of a dimension of $4 \text{ m} \times 4 \text{ m}$. The aquifer is assumed to consist of many facies of glacial sedimentation, which is generally considered as highly heterogeneous (Anderson, 1989). Because of the heterogeneity and difficulties in characterizing the heterogeneity in detail, we conceptualize the heterogeneous T (m^2/day) and S (dimensionless) distributions in the aquifer as stochastic processes, described by mean, variance, and correlation scales (Yeh, 1992; Yeh et al., 2015). The mean of the natural

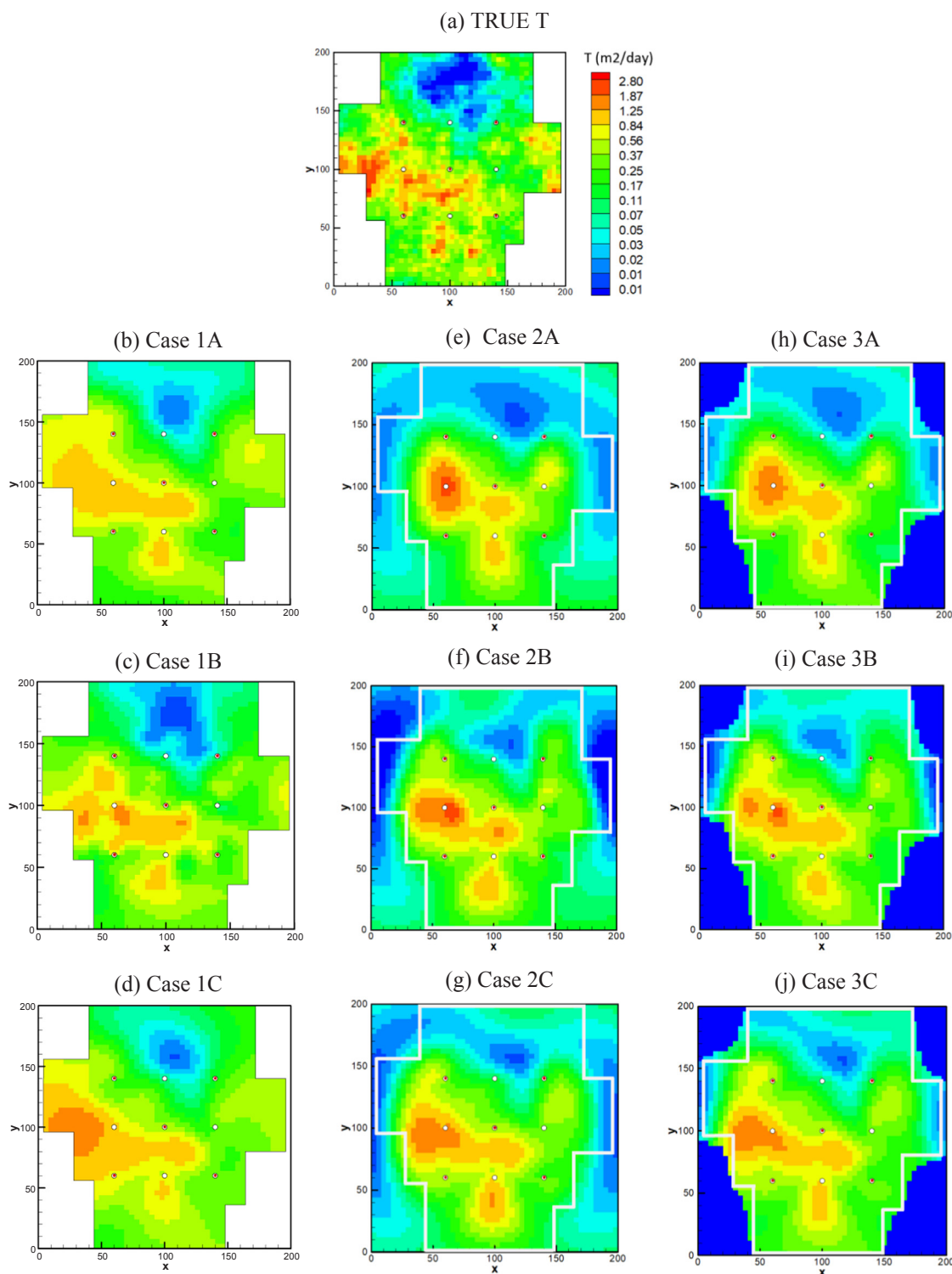


Fig. 2. Contour plots of (a) the true synthetic T field compared to the estimated T of (b, c, d) Case 1, (e, f, g) Case 2, and (h, i, j) Case 3. A, B, and C notation indicate the simulation in a steady-state, a transient state with true S information, and a transient state with uniform S, respectively. Every plot is in the same color scale.

logarithm of T, $\ln T$, and its variance are -1.5 and 1.61 . On the other hand, the mean of the natural logarithm of S, $\ln S$, and its variance are -7.5 and 1.10 . These values represent T and S values of fine sand, silty sand, silt, and glacial till (Heath, 1983; Batu, 1998). The $\ln T$ and $\ln S$ are assumed to be statistically isotropic, with correlation scales of 50 m in x- and y-direction. Based on these spatial statistics, each finite element of the aquifer is assigned a pair of T and S values using a random field generator (Gutjahr, 1989), without considering any correlation

between T and S. Therefore, we have 1,815 different T and S values for the aquifer. The left and right boundaries are no-flow boundaries representing impermeable bedrocks of the valley. The top and bottom boundaries are constant head boundaries of 1000 m. The initial condition is a uniform head of 1000 m. This aquifer with the generated T and S fields and hydraulic conditions (see Fig. 2a and 3a) is our reference aquifer.

Nine wells (the red and the black circles in Fig. 1) are installed in

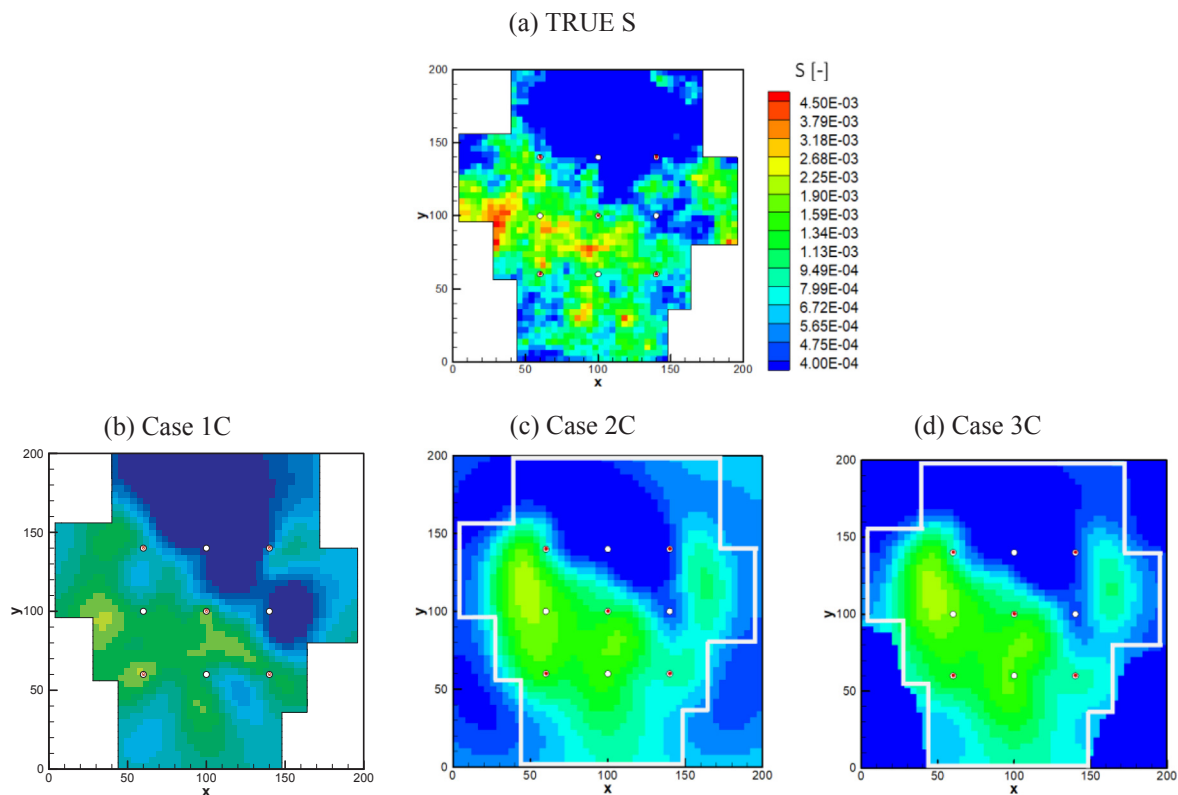


Fig. 3. Contour plots of (a) the true distribution of synthetic S compared to the estimated S of (b) Case 1C, (c) Case 2C, and (d) Case 3C. Every plot is in the same color scale.

the aquifer. Red circles are the wells, used as both pumping and observation wells, and black circles are observation wells. The HT considered here consists of five sequential pumping tests. Each pumping test discharges $30 \text{ m}^3/\text{day}$ of water. In the steady-state simulations, we solve the steady-state form of Eq. (1) with the discharge directly. In the transient simulations, this rate is used to solve the transient form of Eq. (1) over 10 days. After each pumping test, we assume that the aquifer has returned to the initial condition before the next pumping test. We use VSAFT2 (available at www.tian@hwr.arizona.edu) to conduct the forward simulations. The forward simulations yield five sets of drawdown data under steady and transient states.

With the same well-field, the pumping scheme, and aquifer geometry of the reference aquifer, we conduct Monte Carlo forward modeling of HT in ten realizations of the random T and S fields. The simulated drawdown data from each realization of T and S are regarded as the observed HT survey data in the following inverse simulation to derive the estimated T and S fields for each realization.

4. Inverse modeling setups

Using the noise-free steady or transient forward simulation data for each realization, we then investigate the ability of HT to identify the heterogeneity, geometry, and boundaries of the reference field in each realization. Afterward, different prior knowledge of basin geometry, boundary condition, and storage coefficient is applied. The spatial statistics (means, variances, and correlation scales) of the heterogeneity of the reference aquifer is assumed to be known and used in some cases of the inverse modeling exercises. Three cases with different scenarios are examined, and they are defined as follows:

Case 1: In this case, the inverse model uses the correct irregular shape and boundary conditions (Fig. 1a). This case focuses only on the estimated T and S inside the basin, which are not affected by uncertainty in the aquifer shape and boundary conditions.

Case 2: This case considers the situation where the geometry and boundary conditions of the reference aquifer are entirely unknown. To represent this situation, we deliberately assume that the aquifer is a square aquifer ($200 \text{ m} \times 200 \text{ m}$), much larger than the reference aquifer (Fig. 1b). Besides, the four sides of the square aquifer are incorrectly assigned as a constant head boundary (1000 m).

Case 3: This case represents the situation where the partial knowledge of the geometry and boundary conditions of the reference aquifer is available. For example, from the preliminary hydrogeologic investigation, one may know the general geometry and associated low permeability bedrock distribution. To formulate this situation in the inverse model, we first assume a square aquifer ($200 \text{ m} \times 200 \text{ m}$) and then assign a low T value ($10^{-6} \text{ m}^2/\text{d}$) to the areas roughly following the reference aquifer boundaries as the black areas in Fig. 1c.

The above three cases aim to investigate unknown geometry and boundary conditions. Each of the three cases also includes A, B, and C scenarios to investigate the effects of steady-flow and transient flow and different prior information on the estimated parameters. The A, B, and C scenarios are described below.

Scenario A considers the steady-state flow condition, and only the T field is estimated. The inverse model adopts the true mean T over the entire domain in Cases 1, 2, and 3. In Case 3A, the low T zones around the guessed geometry of aquifer are also included as the initial T field.

Scenario B considers the transient-state flow condition in which only T field is estimated while the S field of the reference aquifer is fully prescribed. The initial guess T fields for Case 1, 2, and 3 are the same as those in Scenario A. The known S field in Case 1 is identical to the S field in the reference aquifer. For Case 2, where the domain is larger than that in Case 1, the initial S field is the true S field in the reference aquifer plus an S field with small value (10^{-9}) in the other areas of the square domain. In Case 3, the initial S field is the same as that in Case 2.

Scenario C denotes the situations where the flow is under transient-

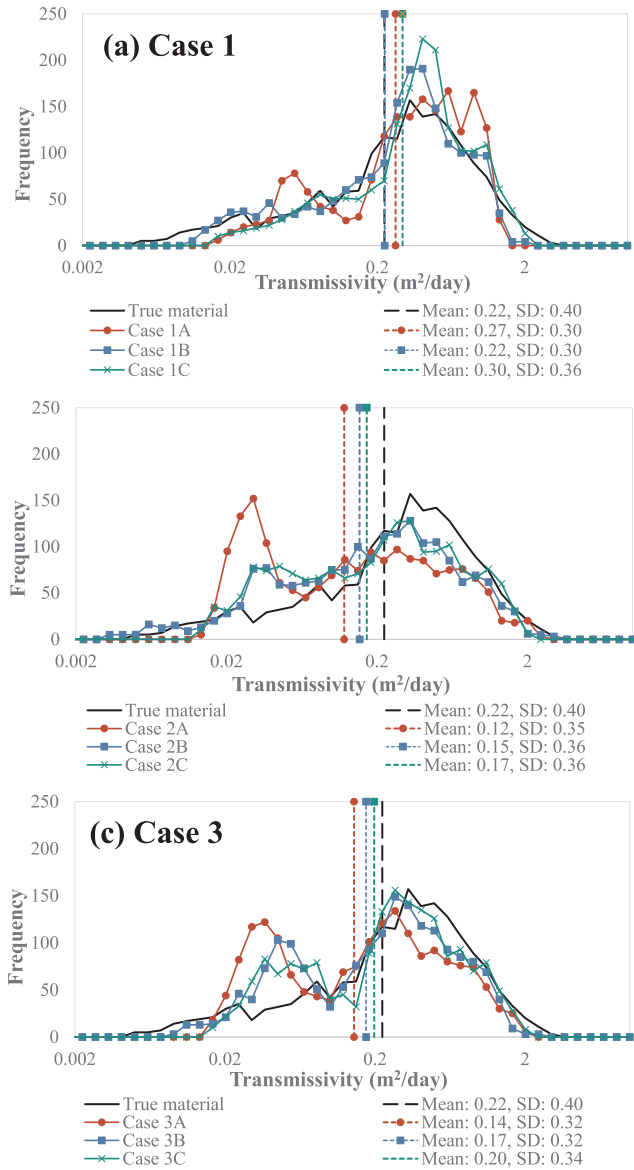


Fig. 4. Distribution of the estimated T in the basin area of (a) Case 1, (b) Case 2, and (c) Case 3. Vertical dashed lines indicate the mean values of each case and scenario.

state conditions, and both T and S fields are estimated with the mean T and S values in all cases.

We conduct the inverse modeling exercise for all cases and scenarios by using the Simultaneous Successive Linear Estimator or SimSLE (Xiang et al., 2009) in VSAFT2. The differences in the variance of the estimated parameter fields and the differences between the observed and simulated head during each consecutive iteration are the criteria for terminating the inverse simulation. The simulation stops reiteration if these criteria are smaller than some specified tolerances.

5. Performance metrics

We use the performance metrics, R^2 , L_1 , L_2 , slope, and intercept from the linear regression analysis of the relationship between reference and estimated hydraulic properties to evaluate the results of the inverse simulations of all the cases. The following equations define these metrics,

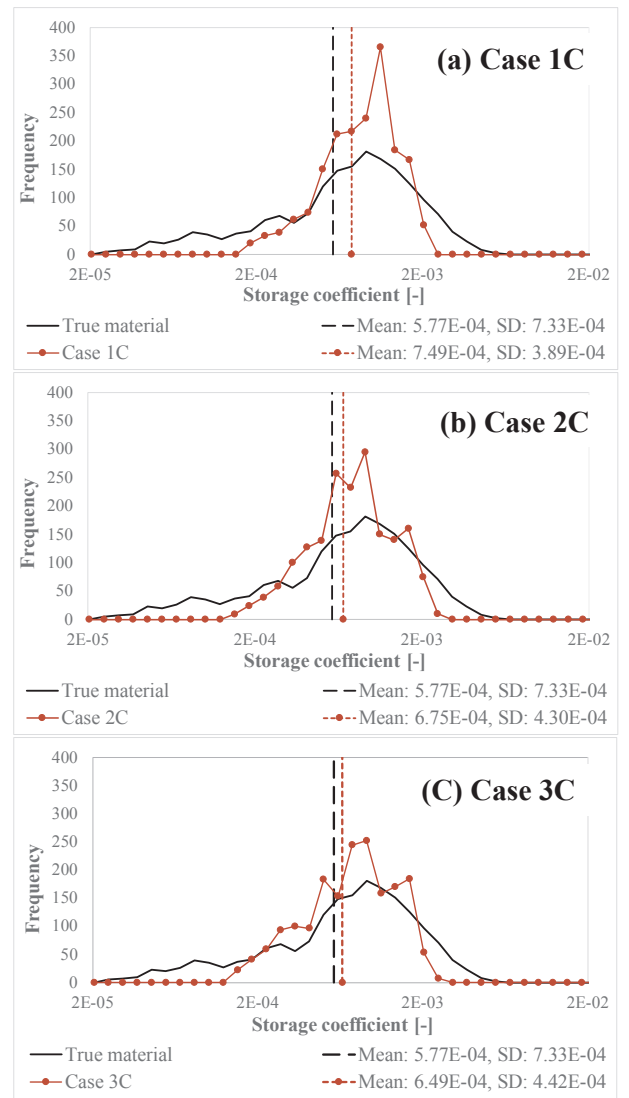


Fig. 5. Distribution of the estimated T in the basin area of (a) Case 1C, (b) Case 2C, and (c) Case 3C. Vertical dashed lines indicate the mean values of each case and scenario.

$$R^2 = \left[\frac{N(\sum x_i \hat{x}_i) - (\sum x_i)(\sum \hat{x}_i)}{\sqrt{[N \sum x_i^2 - (\sum x_i)^2][N \sum \hat{x}_i^2 - (\sum \hat{x}_i)^2]}} \right]^2 \quad (3)$$

$$L_1 = \frac{1}{N} \sum_{i=1}^N |x_i - \hat{x}_i| \quad (4)$$

$$L_2 = \frac{1}{N} \sum_{i=1}^N (x_i - \hat{x}_i)^2 \quad (5)$$

where N is the total number of elements, i is the element number, x_i is the value of T or S at the element i th of the reference field, and \hat{x}_i is the estimated value of T or S at the element i th. Slope and intercept describe the linear equation of the regression line between the estimates and the known values of the parameters in the reference field.

Generally, a small L_1 value means that the mean of the estimated field is close to the mean of the true field, while a small L_2 value indicates the overall deviation of the estimates from the true values is small (i.e., MSE for the prediction of known field). On the other hand, a higher R^2 value suggests a high degree of fit between the regression line and the estimates. Whereas, slope and intercept of the line indicate biasedness of the estimates at every location of the domain. The close to

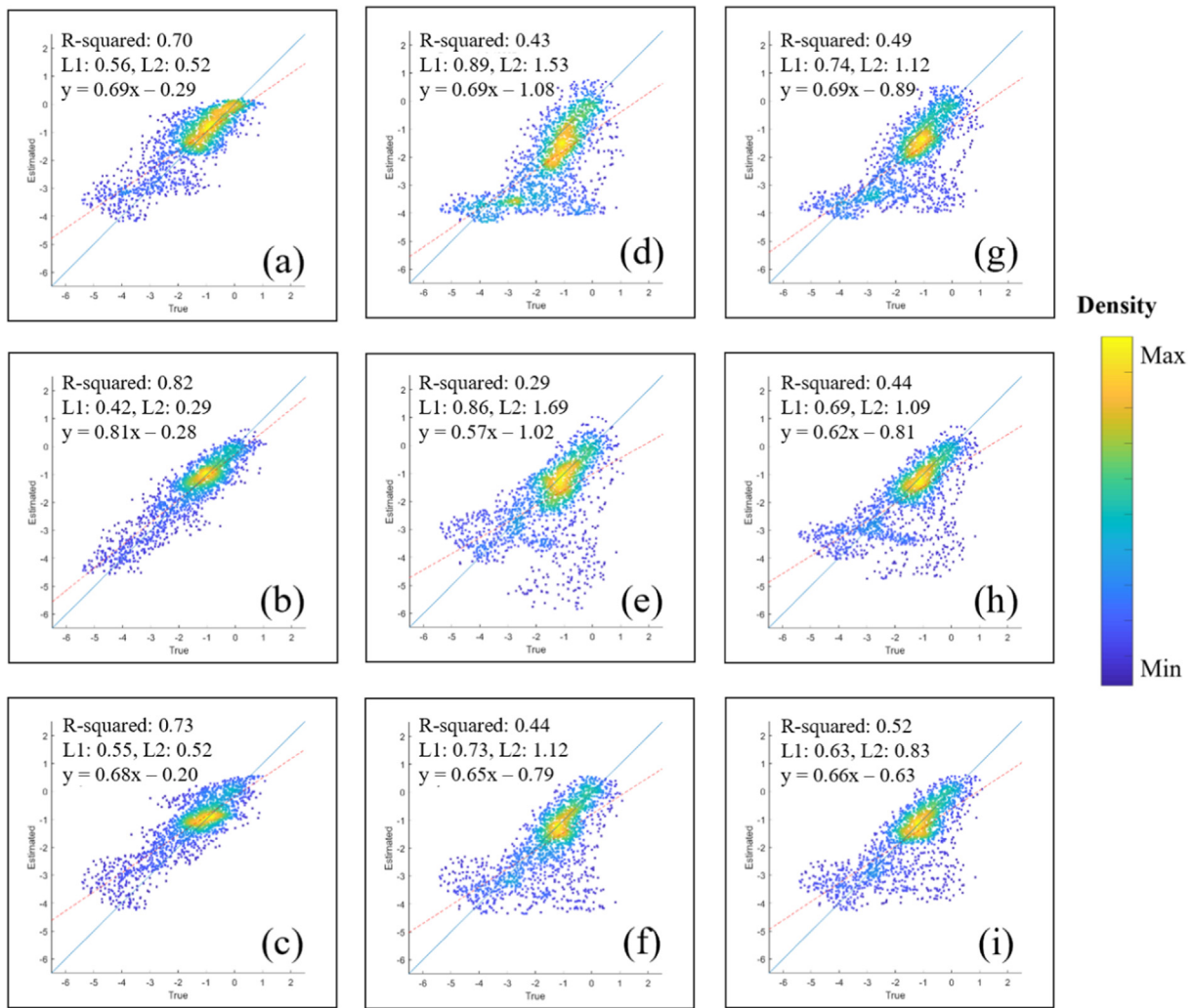


Fig. 6. Scatter plots of true versus estimated T of (a, b, c) Case 1A, 1B, 1C, (d, e, f) Case 2A, 2B, 2C, and (g, h, i) Case 3A, 3B, 3C, respectively, in log scale.

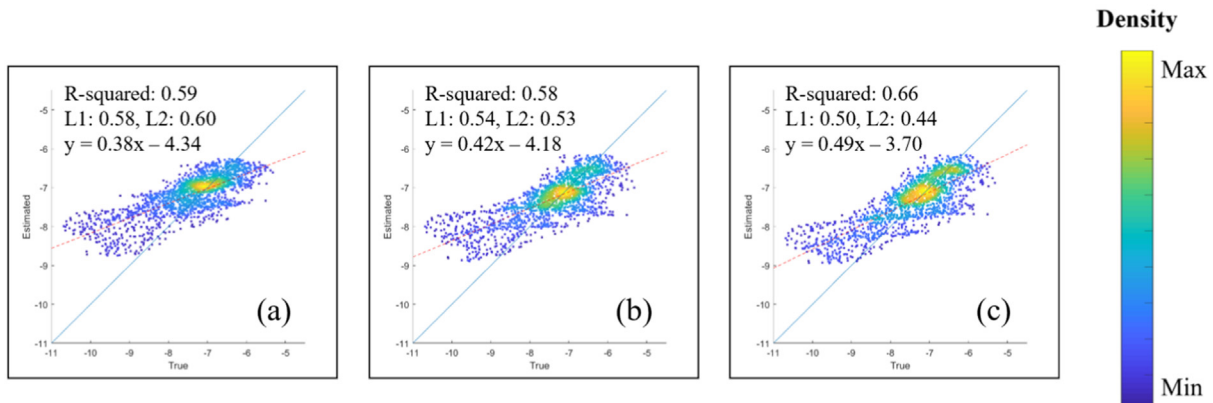


Fig. 7. Scatter plots of true versus estimated S of (a) Case 1C, (b) Case 2C, and (c) Case 3C in log scale.

1 and zero, respectively, they are, the estimates are less biased.

6. Results and discussions

In this section, we discuss the HT inverse results of Cases 1, 2, and 3, with A, B, and C scenarios first. Then, the discussion of the results of Monte Carlo simulation follows.

6.1. Single realization

Results of the single realization experiments are presented as contour maps, histograms, and scatter plots.

7. Contour Maps.

T estimates. The true distribution of the T field and boundary

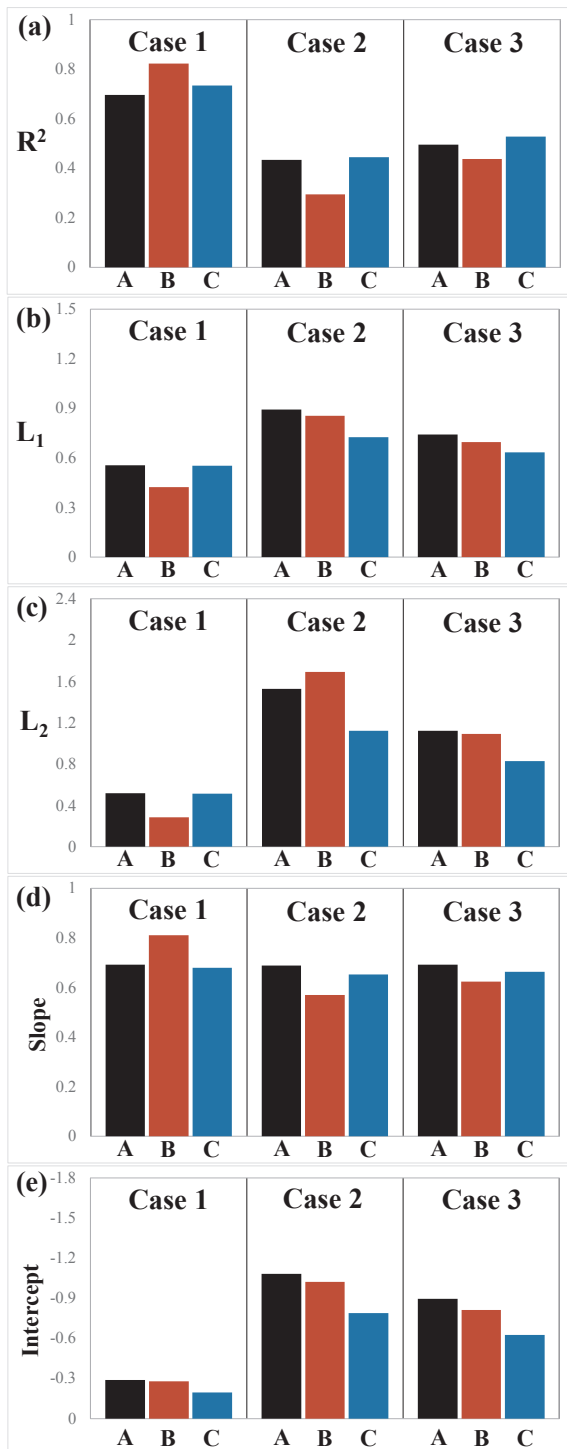


Fig. 8. The calculated mean of one realization of estimated T performance metrics: (a) R², (b) L₁, (c) L₂, (d) slope, (e) intercept, in log scale.

geometry of the synthetic aquifer are depicted in Fig. 2a. Again, Case 1 denotes the situation where the exact aquifer geometry is known. In this case, the contour maps of the estimated T fields using steady-state heads (Case 1A) is illustrated in Fig. 2b. Fig. 2c shows the T estimates, using transient heads and complete knowledge of S field (i.e., Case 1B). The estimated T field using the transient head data with the mean S (i.e., Case 1C) is displayed in Fig. 2d. These figures under Case 1 present the best estimates with the exact aquifer geometry and boundary conditions. These best estimates, thus, are the basis for comparing results of Cases 2A, 2B, and 2C (the geometry is completely unknown) as well as

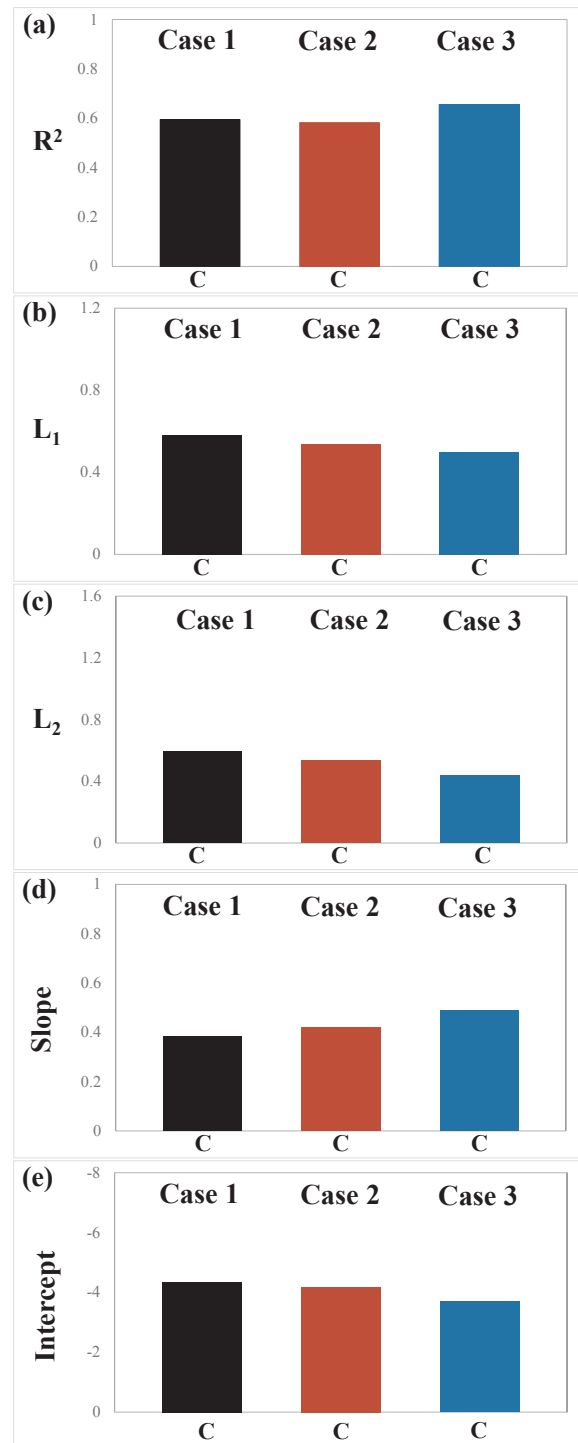


Fig. 9. The calculated mean of one realization of estimated S performance metrics: (a) R², (b) L₁, (c) L₂, (d) slope, (e) intercept, in log scale.

Cases 3A, 3B, 3C (where the geometry is partially known).

Visual comparisons of the contour maps of the estimated T fields for all cases and scenarios with that of the reference aquifer (Fig. 2a) indicate that the estimated T fields all capture the general trend of the true one. However, the estimates from Case 1 (with the known geometry and boundary) under A, B, and C scenarios are closer to the true T field than are those in Cases 2 and 3, where the geometry and boundary are incompletely specified.

Examining Cases 1A, 1B, and 1C, we observed that in Case 1B, the estimated T field seems to have more detailed irregular patterns

Table 1
Performance metrics in the log scale of the estimated T from ten realizations.

Performance Metrics	Scenarios	Case 1		Case 2		Case 3	
		Mean	SD	Mean	SD	Mean	SD
R ²	A	0.67	0.07	0.46	0.09	0.49	0.10
	B	0.76	0.10	0.44	0.11	0.50	0.10
	C	0.69	0.09	0.50	0.13	0.55	0.12
L ₁	A	0.56	0.07	0.91	0.14	0.78	0.12
	B	0.48	0.09	0.79	0.10	0.71	0.11
	C	0.57	0.10	0.74	0.12	0.66	0.11
L ₂	A	0.54	0.13	1.46	0.36	1.12	0.30
	B	0.40	0.17	1.34	0.31	1.04	0.21
	C	0.56	0.18	1.04	0.27	0.79	0.22
Slope	A	0.67	0.10	0.69	0.11	0.66	0.11
	B	0.76	0.10	0.72	0.12	0.71	0.10
	C	0.69	0.11	0.70	0.12	0.65	0.12
Intercept	A	-0.39	0.15	-0.99	0.39	-0.91	0.21
	B	-0.33	0.13	-0.78	0.17	-0.67	0.15
	C	-0.23	0.13	-0.71	0.15	-0.63	0.13

(localized high/low T areas) than those of Case 1A and 1C. Again, Case 1B is the case where the transient data and precise S distribution are used. Case 1A, where only the steady-state head is used in the inverse modeling exercise. Case 1C uses the transient head data but the mean S field. The irregular details in Case 1B seem to suggest that using the transient head data with the true S field can obtain a better estimated T field. That is, the transient head data may carry more information about the T heterogeneity than the steady-state head data. However, after a close examination, we find that the locations of the high/low T areas do not necessarily coincide with those in the true T field.

As a consequence, it is difficult to certify the superiority of Case 1B to Case 1A and Case 1C. Likewise, it is difficult to distinguish the performance of HT using steady-state data and that using transient head and the mean S. While the T estimates in Case 1A and Case 1C are smooth, they are still in good agreement with the true T field of the reference aquifer. This paradox likely stems from the fact that these inverse problems are ill-defined or under-determined, and there are many possible estimates.

Despite the entirely unknown geometry and incorrect boundary conditions, the estimated T fields in Cases 2A, B, and C can roughly depict the true geometry (outlined by the white lines) using zones of low T values around the true geometry. Examination of the estimates in Cases 3A, 3B, and 3C seems to indicate that with the partial knowledge of geometry and boundary conditions, HT yields similar results as those with entirely unknown geometry and boundary conditions (Cases 2A, 2B, and 2C).

Overall, these results suggest that the exact knowledge of geometry and boundary conditions in HT analysis could lead to better-estimated T fields in the aquifer using either steady-state or transient data (Case 1). They also show that the partial knowledge of geometry and boundary conditions (Cases 3A, B, and C) does not make any significant improvement of the T estimates.

S estimates. The true distribution of the S field and boundary geometry of the synthetic aquifer are depicted in Fig. 3a. Fig. 3b, c, and d illustrate the contour maps of the estimated S fields for Case 1C, Case 2C, and Case 3C. Notice that Scenarios A and B of Cases 1, 2, and 3 do not estimate S field, and they are excluded here.

Comparing Fig. 3a, b, c, and d, the estimated S fields in Cases 1C, 2C, and 3C, we observe that the estimated S fields have very similar patterns as that of the true S field. None of the estimated fields, however, can capture the detailed high value S distribution of the true field, even if the geometry and boundary conditions are known precisely (Fig. 3b). Again, using the completely different geometry and incorrect constant head boundary conditions, HT estimates (Case 2C) reflect the general geometry and boundary condition by low S zones.

That is to say, using the HT survey and SimSLE, one can detect the

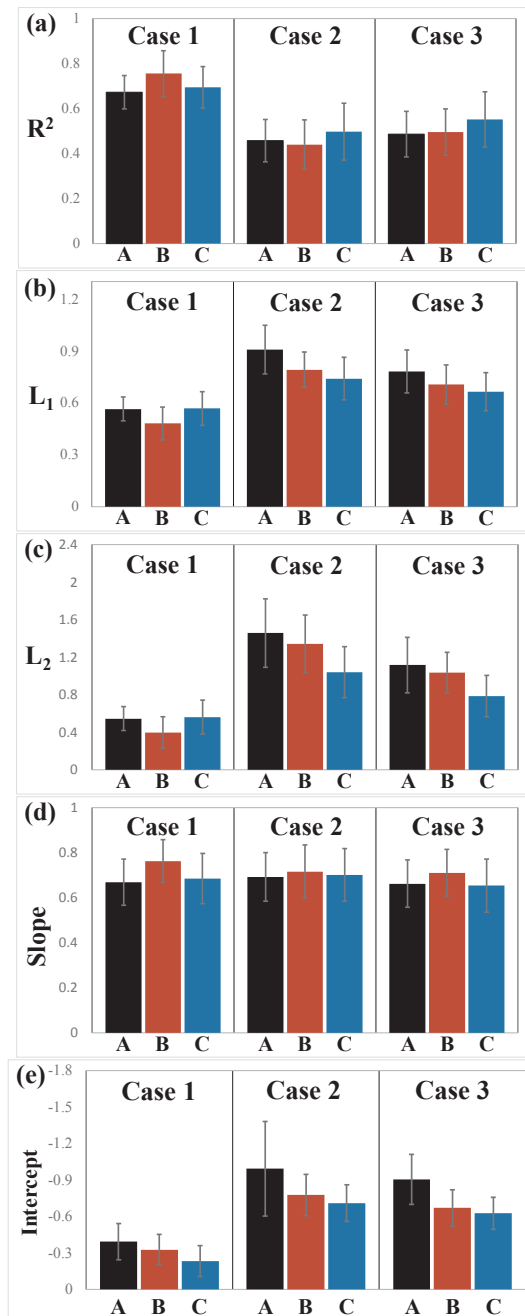


Fig. 10. The calculated mean and standard deviation over ten realizations of estimated T performance metrics: (a) R², (b) L₁, (c) L₂, (d) slope, (e) intercept, in log scale. The vertical line denotes the standard deviation.

Table 2
Performance metrics in the log scale of the estimated S from ten realizations.

Performance Metrics	Scenarios	Case 1		Case 2		Case 3	
		Mean	SD	Mean	SD	Mean	SD
R ²	C	0.65	0.10	0.59	0.11	0.60	0.12
L ₁	C	0.52	0.09	0.53	0.08	0.60	0.26
L ₂	C	0.46	0.17	0.47	0.13	0.64	0.61
Slope	C	0.54	0.14	0.54	0.11	0.45	0.32
Intercept	C	-3.26	0.94	-3.35	0.75	-4.00	2.35

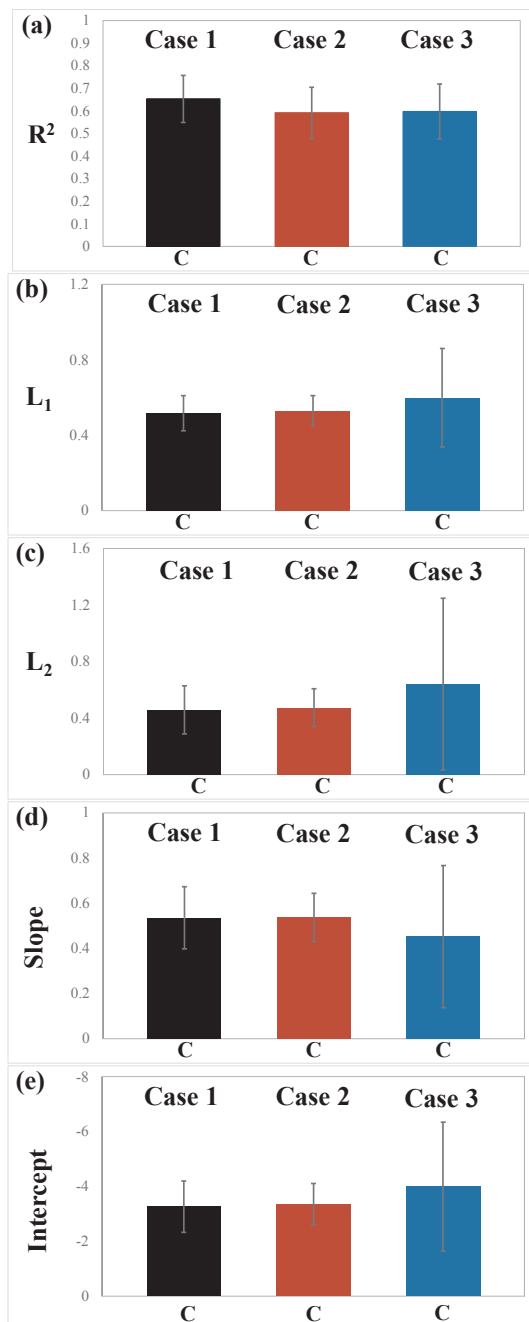


Fig. 11. The calculated mean and standard deviation over ten realizations of estimated S performance metrics: (a) R^2 , (b) L_1 , (c) L_2 , (d) slope, (e) intercept, in log scale. The vertical line denotes the standard deviation.

impermeable boundary and its geometry and the general pattern of the heterogeneity inside the aquifer, even if the geometry and boundary conditions are not available.

8. Histograms

As another way to evaluate estimated T and S of the aquifer, histogram plots of the true and estimated T values for Cases 1A, B, and C are presented in Fig. 4a. For Cases 2A, B, and C, they are in Fig. 4b, and Cases 3A, B, and C are in Fig. 4c. Histograms of scenarios A, B, and C in these three cases are shown with different color lines along with the actual distribution (solid black line).

According to the figures, while the histograms in Cases 1A, B, and C are similar to the true one, those of the estimated T fields in Case 2 and

Case 3 for all scenarios exhibit two distinct peaks. The second peaks at low T values represent the estimated T values at regions close to the impermeable boundary of the actual field. These peaks indicate that even though the true impermeable geometry is unknown, HT with an incorrect geometry with constant head boundaries will assign low T zones near the true impermeable boundaries.

Notice that the true mean of T of the synthetic aquifer is $0.22 \text{ m}^2/\text{day}$, and the mean of the estimates of Case 1B is closest to the true one with a value of $0.22 \text{ m}^2/\text{day}$. The one that has the most significant difference is the mean of the estimated T of Case 2A, which has a value of $0.12 \text{ m}^2/\text{day}$. These results indicate that the unknown impermeable geometry of the aquifer affects the mean values of the T estimates, creating some bias of the estimates.

The histograms of the estimated S fields for Case 1C, Case 2C, and Case 3C are shown in Fig. 5a, b, and c, respectively. The distributions of the S estimates in all cases exhibit only one peak, resembling the peak of the true one. These figures also show the mean and standard deviation of the true and estimated S field. The distributions of the estimates for the three cases are narrower than the true S field (as indicated by the standard deviations), although they are similar. This finding may suggest that 1) S estimates are not sensitive to the geometry and boundary of the aquifer, and 2) detailed S distribution is difficult to estimate.

9. Scatter plots

Scatter plots in Figs. 6 and 7 show the relationships between the estimates and true T and S values, respectively. Colors of scatter plots represent different data accumulation density; the light-yellow color denotes the highest density, while the dark blue color indicates the lowest density, as shown in the color bars on the right side of the figures. These figures also include the values of R^2 , L_1 , and L_2 , in addition to the slope and intercept of the regression line.

According to Fig. 6, we observe the following. The estimated T fields based on the correct geometry and boundary conditions (Cases 1A, B, and C) have higher R^2 and smaller L_1 and L_2 values than those of all scenarios in other cases. Comparing the scatter plots and the performance metrics of A, B, and C scenarios in Case 1, it is apparent that the T estimates from Scenario B outperform those in Scenarios A and C. That is, with exact geometry and boundary conditions, HT using transient data and the exact S field to estimate T field yields the best result. Again, HT using the steady-state data (Scenario A) performs equally well, comparing to Scenario C, where the transient data and the mean S are used to estimate both T and S fields.

In Cases 2 and 3, data points tend to scatter significantly from the 1:1 line when the inverse model uses incorrect geometry and boundary conditions. The intercept values of all cases are negative, and slope values are less than one. These slope values indicate that some bias in the estimated T values at some locations owing to the limited amount of spatial observation data. Generally, the estimated T fields reproduce the major trends of high and low T zones of the true T field, with some scattering around from the actual values.

The scatter plots of the S fields (Fig. 7A, B, and C) show the same trend in every case without significant differences among the three cases compared to the scatter plots of T. The values of R^2 of Case 1, Case 2, and Case 3 are 0.59, 0.58, and 0.66, and L_2 is 0.60, 0.53, and 0.44, respectively. The slopes of the regression lines for S scatter plots (Fig. 7) are smaller than those of T scatter plots (Fig. 6).

These results are indicative of the fact that HT can identify less variation of S values than the variation of T values. The reason is that the cross-correlation between head and S is restricted to the narrow region between the observations well and the pumping well (Sun et al., 2013).

10. Summary of results of single realization

The values of R^2 , L_1 , L_2 , slope, and intercept of the linear regression relationship between T and S estimates and the reference ones for all cases and scenarios are summarized as bar charts in Figs. 8 and 9. According to these bar charts, we may conclude that in this one realization, all scenarios in Case 1, when geometry and boundary conditions are known, have the best T estimates among all the cases. In addition, HT using transient data and exact S field (Case 1B) gives the best estimate of the T field. The estimates from Case 1A (steady-state data) and Case 1C (transient data with the mean S) are similar.

The differences in the performances of Case 2 and Case 3 is minor, and there is no consistent metrics to evaluate these two cases. Although the slope in Case 2 seems to be the same as that in Case 3, other metrics indicate that estimates in Case 3 is slightly better than those in Case 2. The differences in the performance metric of S estimates, as illustrated in Fig. 9, are even smaller than those in Fig. 8. Interestingly, Case 3 (estimates using partial knowledge of the geometry and boundaries) seems to have the best performance metrics, even better than those in Case 1. Such a counterintuitive result may suggest results from one single realization inconclusive.

10.1. Monte Carlo simulation

Because the inverse problem is ill-defined or under-determined, there are many possible solutions, results of inverse modeling based on one single realization could be misleading or inconclusive. The results of the Monte Carlo simulation could address this issue.

Table 1 lists the average and standard deviation of R^2 , L_1 , L_2 , slope, and intercept of the estimated T of each case and A, B, and C scenarios, resulting from MC simulations using ten realizations. Fig. 10 illustrates the mean of these values as bar charts and the standard deviation as vertical bars for better visualization. From the standard deviation bars of R^2 , L_1 , and L_2 values, we observe that the performance of the estimates varies from one realization to another realization. However, the means of these performance metrics for the ten realizations suggest that the simulation of Case 1 results in the highest R^2 , lowest L_1 and L_2 , and smallest intercepts, which indicate the smallest discrepancy of the estimates from the actual values. However, its slopes are similar to those of Cases 2, and 3.

Among A, B, and C scenarios in Case 1 (exact geometry and boundary conditions), the means of the performance metrics indicate that HT using transient head data with the exact S field produces the best-estimated T field. Similar to the results of one single realization, the performance metrics of Scenarios A (steady-state head) and C (transient head with the mean S) are indistinguishable.

We can thus conclude that complete knowledge of the geometry and boundary conditions enhance the resolution of the estimates of the T field in the aquifer. Similar to the situation in one single realization, differences in these performance metrics between Cases 2 and 3 are minute. Slightly better R^2 , L_1 , L_2 , and intercept values indicate that the T estimates are better when partial geometry and boundary are known. The similar slope values between all cases imply that the estimates have depicted the general patterns of the heterogeneity in the aquifer.

Similarly, Table 2 and Fig. 11 display the average and standard deviation of the performance metrics of the estimated S in all cases. According to the average of the performance metrics from the ten realizations, the estimated S using the correct boundary model (Case 1C) results in the highest R^2 of 0.65 and the smallest L_1 , L_2 , among all of the cases. Nevertheless, differences in R^2 values of the estimated S among the three cases are slight. Despite the small difference, values of the average R^2 , L_1 , L_2 , slope, and intercept of Cases 2 are noticeably better than those of Case 3. This result is different from that based on one realization (Fig. 9). Results from one single realization indicate Case 3 (partial knowledge of the geometry and boundary) yields better estimates than Case 2 (completely unknown geometry). Future studies

should investigate these puzzles.

Summary. Overall, the performance metrics vary from one realization to another. Nevertheless, performance metrics averaged over the results of MC experiments suggest that with the knowledge of the exact geometry and boundary conditions, HT with transient head data and using a fully specified heterogeneous S field (Case 1B) can yield the best-estimated T field. Meanwhile, HT using transient head data with a correct mean S field to estimate both T and S fields (Case 1C) produces a slightly better estimated T field than HT using the steady-state head data (Case 1A). This finding seems to suggest that transient head data may carry more information about the T heterogeneity than the steady-state head data. The usefulness of the additional information, yet, becomes in vain as the number of unknowns to be sought increases. The similarity in the results of Case 1C and Case 1A appears to support this explanation.

11. Conclusions

With incorrect guess constant head boundary conditions, HT identifies the impermeable boundaries as lower T zones in the vicinity of the boundary. These estimated low T zones generally outline the irregular shape of the impermeable boundary of the aquifer. Estimated S shows these characteristics of low S zones as well.

The comparison of the estimates inside the aquifer in every case leads to the conclusion that boundary conditions are essential to parameter estimation. The case with correct boundary geometries and conditions (Case 1) always results in a better estimation of T and S. The zonation of the initial guesses of T and S based on prior knowledge of geology improves the estimation compared to the case using only the mean properties of the aquifer. Using the correct S field as the prior information improves the estimation only in the case that boundary geometries and conditions are correctly defined (Case 1). On the contrary, using the average value of S yields a better estimation in the cases with incorrect boundary geometries and conditions (Case 2 and Case 3).

For practical purposes, we suggest that, in any case, one should always employ HT survey to collect non-redundant information as much as possible (i.e., conducting many sequential pumping tests). Then, one should delineate the geometry based on geological information, set the boundaries as constant head boundaries to conduct HT analysis. The HT estimates will correct the constant head boundaries to low permeable zones or high permeable zones near the boundaries to reflect actual boundary conditions. As sufficient HT data are collected, the estimates from HT analysis will enhance the estimates in the aquifer and near its boundaries. Of course, geologic, geophysical information, and others should be used as prior information (soft constraints) for HT inversion.

The future study should consider MCS with more than 10 realizations as well as a range of mean, variance, and correlation scale values. Nonetheless, this study shows that the means and standard deviations of performance metrics from MCS are necessary to evaluate the results of an inverse problem. These statistics could draw a definitive conclusion of the experiment. This result is a significant contribution to the inverse modeling of ill-defined problems.

CRediT authorship contribution statement

Kwankwai Daranond: Conceptualization, Methodology, Formal analysis, Writing - original draft, Visualization. **Tian-Chyi Jim Yeh:** Writing - original draft, Writing - review & editing, Supervision. **Yonghong Hao:** Writing - review & editing. **Jet-Chau Wen:** Writing - review & editing. **Wenke Wang:** Writing - review & editing.

Declaration of Competing Interest

The authors declare that they have no known competing financial

interests or personal relationships that could have appeared to influence the work reported in this paper.

Acknowledgment

The first author acknowledges the support of the scholarship from the Royal Thai Government and the Department of Groundwater Resources, Thailand. This study is also partially supported by the U.S. NSF grant EAR1931756.

References

- Anderson, M.P., 1989. Hydrogeologic facies models to delineate large-scale spatial trends in glacial and glaciofluvial sediments. *Geol. Soc. Am. Bull.* 101 (4), 501–511. [https://doi.org/10.1130/0016-7606\(1989\)101](https://doi.org/10.1130/0016-7606(1989)101).
- Batu, V., 1998. *Aquifer Hydraulics: A Comprehensive Guide to Hydrogeologic Data Analysis*. Wiley, New York.
- Berg, S.J., Illman, W.A., 2015. Comparison of hydraulic tomography with traditional methods at a highly heterogeneous site. *Groundwater* 53 (1), 71–89. <https://doi.org/10.1111/gwat.12159>.
- Berg, S., Illman, W., 2013. Field study of subsurface heterogeneity with steady-state hydraulic tomography. *Ground Water* 51 (1), 29–40.
- Berg, S.J., Illman, W.A., 2011. Capturing aquifer heterogeneity: comparison of approaches through controlled sandbox experiments. *Water Resour. Res.* 47 (9). <https://doi.org/10.1029/2011wr010429>.
- Bohling, G., Butler, J., 2010. Inherent limitations of hydraulic tomography. *Ground Water* 48 (6), 809–824.
- Cardiff, M., Bakhos, T., Kitanidis, P.K., Barrash, W., 2013. Aquifer heterogeneity characterization with oscillatory pumping: sensitivity analysis and imaging potential. *Water Resour. Res.* 49, 5395–5410. <https://doi.org/10.1002/wrcr.20356>.
- Cardiff, M., Barrash, W., Kitanidis, P., 2012. A field proof-of-concept of aquifer imaging using 3-D transient hydraulic tomography with modular, temporarily-employed equipment. *Water Resour. Res.* 48 (5).
- Cardiff, M., Barrash, W., 2011. 3-D transient hydraulic tomography in unconfined aquifers with fast drainage response. *Water Resour. Res.* 47 (12).
- Cardiff, M., Barrash, W., Thoma, M., Malama, B., 2011. Information content of slug tests for estimating hydraulic properties in realistic, high-conductivity aquifer scenarios. *J. Hydrol.* 403 (1–2), 66–82. <https://doi.org/10.1016/j.jhydrol.2011.03.044>.
- Castagna, M., Becker, M.W., Bellin, A., 2011. Joint estimation of transmissivity and storativity in a bedrock fracture. *Water Resour. Res.* 47 (9). <https://doi.org/10.1029/2010wr009262>.
- Cooper, H., Jacob, C., 1946. A generalized graphical method for evaluating formation constants and summarizing well-field history. *Trans. Am. Geophys. Union* 27 (4), 526.
- Gutjahr, A.L., 1989. Fast fourier transforms for random field generation: project report for Los Alamos Grant to New Mexico Tech. New Mexico Institute of Mining and Technology, Socorro, NM.
- Heath, R.C., 1983. Basic ground-water hydrology. doi: 10.3133/wsp2220.
- Huang, S.-Y., Wen, J.-C., Yeh, T.-C.J., Lu, W., Juan, H.-L., Tseng, C.-M., Lee, J.-H., Chang, K.-C., 2011. Robustness of joint interpretation of sequential pumping tests: Numerical and field experiments. *Water Resour. Res.* 47 (10). <https://doi.org/10.1029/2011wr010698>.
- Illman, W., Berg, S., Zhao, Z., 2015. Should hydraulic tomography data be interpreted using geostatistical inverse modeling? A laboratory sandbox investigation. *Water Resour. Res.* 51 (5), 3219–3237.
- Illman, W.A., Liu, X., Takeuchi, S., Yeh, T.-C.J., Ando, K., Saegusa, H., 2009. Hydraulic tomography in fractured granite: Mizunami Underground Research site, Japan. *Water Resour. Res.* 45 (1). <https://doi.org/10.1029/2007wr006715>.
- Li, K., Zhang, Y., Yeh, T.-C.J., Zhao, L., Su, X., Wang, Y.-L., Qi, Y., 2019. An iterative scheme to map and incorporate geologic information of discontinuous heterogeneity in hydraulic tomography. *J. Hydrol.* 579, 124143. <https://doi.org/10.1016/j.jhydrol.2019.124143>.
- Liu, S., Yeh, T. and Gardiner, R. (2002). Effectiveness of hydraulic tomography: Sandbox experiments. *Water Resources Research*, 38(4), pp.5-1-5-9.
- Liu, X., Illman, W.A., Craig, A.J., Zhu, J., Yeh, T.-C.J., 2007. Laboratory sandbox validation of transient hydraulic tomography. *Water Resour. Res.* 43 (5). <https://doi.org/10.1029/2006wr005144>.
- Lu, C., Chen, Y., Luo, J., 2012. boundary condition effects on maximum groundwater withdrawal in coastal aquifers. *Ground Water* 50 (3), 386–393. <https://doi.org/10.1111/j.1745-6584.2011.00880.x>.
- Ni, C., Yeh, T., Chen, J., 2009. Cost-effective hydraulic tomography surveys for predicting flow and transport in heterogeneous aquifers. *Environ. Sci. Technol.* 43 (10), 3720–3727.
- Straface, S., Yeh, T., Zhu, J., Troisi, S., Lee, C., 2007. Sequential aquifer tests at a well field, Montalto Uffugo Scalo, Italy. *Water Resour. Res.* 43 (7).
- Sun, R., Yeh, T.-C.J., Mao, D., Jin, M., Lu, W., Hao, Y., 2013. A temporal sampling strategy for hydraulic tomography analysis. *Water Resour. Res.* 49, 3881–3896. <https://doi.org/10.1002/wrcr.20337>.
- Theis, C., 1935. The relation between the lowering of the Piezometric surface and the rate and duration of discharge of a well using ground-water storage. *Trans. Am. Geophys. Union* 16 (2), 519.
- Tiedeman, C.R., Barrash, W., 2019. Hydraulic tomography: 3D hydraulic conductivity, fracture network, and connectivity in mudstone. *Groundwater*. <https://doi.org/10.1111/gwat.12915>.
- Tso, M.C., Zha, Y., Yeh, T., Wen, J., 2016. The relative importance of head, flux, and prior information in hydraulic tomography analysis. *Water Resour. Res.* 52 (1), 3–20.
- Wang, Y.L., Yeh, T.-C.J., Wen, J.C., Gao, X., Zhang, Z., Huang, S.Y., 2019. Resolution and ergodicity issues of river stage tomography with different excitations. *Water Resour. Res.* <https://doi.org/10.1029/2018wr023204>.
- Wen, J., Chen, J., Yeh, T., Wang, Y., Huang, S., Tian, Z., Yu, C., 2019. Redundant and Nonredundant Information for Model Calibration or Hydraulic Tomography. *Groundwater*.
- Wen, J., Wu, C., Yeh, T., Tseng, C., 2010. Estimation of effective aquifer hydraulic properties from an aquifer test with multi-well observations (Taiwan). *Hydrogeol. J.* 18 (5), 1143–1155.
- Wu, C.-M., Yeh, T.-C.J., Zhu, J., Lee, T.H., Hsu, N.-S., Chen, C.-H., Sancho, A.F., 2005. Traditional analysis of aquifer tests: comparing apples to oranges? *Water Resour. Res.* 41 (9). <https://doi.org/10.1029/2004wr003717>.
- Xiang, J., Yeh, T.J., Lee, C., Hsu, K., Wen, J., 2009. A simultaneous successive linear estimator and a guide for hydraulic tomography analysis. *Water Resour. Res.* 45 (2). <https://doi.org/10.1029/2008wr007180>.
- Yeh, T., Khaleel, R., Carroll, K.C., 2015. *Flow Through Heterogeneous Geological Media*. Cambridge University Press, Cambridge.
- Yeh, T., Lee, C., 2007. Time to change the way we collect and analyze data for aquifer characterization. *Ground Water* 45 (2), 116–118.
- Yeh, T., Liu, S., 2000. Hydraulic tomography: Development of a new aquifer test method. *Water Resour. Res.* 36 (8), 2095–2105.
- Yeh, T., Srivastava, R., Guzman, A., Harter, T., 1993. A numerical model for water flow and chemical transport in variably saturated porous media. *Ground Water* 31 (4), 634–644.
- Yeh, T., 1992. Stochastic modeling of groundwater flow and solute transport in aquifers. *Hydrol. Process.* 6 (4), 369–395.
- Yin, D., Illman, W., 2009. Hydraulic tomography using temporal moments of drawdown recovery data: a laboratory sandbox study. *Water Resour. Res.* 45 (1).
- Zha, Y., Yeh, T., Illman, W., Onoe, H., Mok, C., Wen, J., Huang, S., Wang, W., 2017. Incorporating geologic information into hydraulic tomography: a general framework based on geostatistical approach. *Water Resour. Res.* 53 (4), 2850–2876.
- Zha, Y., Yeh, T., Illman, W., Tanaka, T., Bruines, P., Onoe, H., Saegusa, H., Mao, D., Takeuchi, S., Wen, J., 2016. An application of hydraulic tomography to a large-scale fractured granite site, Mizunami, Japan. *Groundwater* 54 (6), 793–804.
- Zhao, Z., Illman, W.A., 2018. Three-dimensional imaging of aquifer and aquitard heterogeneity via transient hydraulic tomography at a highly heterogeneous field site. *J. Hydrol.* 559, 392–410. <https://doi.org/10.1016/j.jhydrol.2018.02.024>.
- Zhao, Z., Illman, W.A., 2017. On the importance of geological data for three-dimensional steady-state hydraulic tomography analysis at a highly heterogeneous aquifer-aquitard system. *J. Hydrol.* 544, 640–657. <https://doi.org/10.1016/j.jhydrol.2016.12.004>.
- Zhao, Z., Illman, W.A., Berg, S.J., 2016. On the importance of geological data for hydraulic tomography analysis: Laboratory sandbox study. *J. Hydrol.* 542, 156–171. <https://doi.org/10.1016/j.jhydrol.2016.08.061>.
- Zhu, J., Yeh, T., 2005. Characterization of aquifer heterogeneity using transient hydraulic tomography. *Water Resour. Res.* 41 (7).